Characteristic analysis of a complex two-dimensional magnetohydrodynamic bow shock flow with steady compound shocks

H. De Sterck[a] and B. C. Low
High Altitude Observatory, National Center for Atmospheric Research, P.O. Box 3000, Boulder, Colorado 80307-3000

S. Poedts[b]
Centre for Plasma Astrophysics, Katholieke Universiteit Leuven, Celestijnenlaan 200B, 3001 Leuven, Belgium

(Received 22 September 1998; accepted 24 November 1998)

A simple, compact, and systematic derivation is given of the characteristic properties of the magnetohydrodynamic (MHD) equations with two independent variables (time-dependent MHD in the xt plane and steady MHD in the xy plane), based on the symmetrizable Galilean invariant form of the equations and using a matrix approach. A numerically obtained stationary planar field-aligned MHD bow shock flow with interacting shocks is then analyzed in terms of hyperbolic and elliptic regions, steady xy characteristics, limiting lines, and allowed shock transitions. With the help of this analysis, a wave structure present in the bow shock flow can be interpreted as a double steady compound shock. This interpretation is based on the complete analogy demonstrated in our analysis, between the xy characteristic structure of this novel steady compound shock and the xt characteristic structure of the well-known time-dependent MHD compound shock. © *1999 American Institute of Physics.* [S1070-664X(99)01103-9]

I. INTRODUCTION

The equations of ideal magnetohydrodynamics[1] (MHD) are widely used to model plasma flows in astrophysics[2–6] and laboratory plasma physics.[7–9] This system of equations belongs to the class of symmetric hyperbolic systems,[10] which have many interesting and well-defined properties. Ideal MHD allows for three linear wave modes, the fast magnetosonic, the Alfvén, and the slow magnetosonic wave, with (positive) anisotropic wave speeds satisfying $c_f \geqslant c_A \geqslant c_s$ in standard notation. Nonlinear interaction of these different wave modes can lead to the formation of a wealth of shocks and discontinuities.[1,11–13]

An extensive general theory exists for the characteristic properties of symmetric hyperbolic systems.[10,14] This theory has been applied early on to unsteady MHD flows[10] and to steady planar ($B_z \equiv 0$ and $v_z \equiv 0$) MHD flows, including the case where the magnetic field is aligned with the flow (field-aligned or parallel flow).[15,16] More complete accounts of the characteristic theory of steady and unsteady MHD flows appeared later.[17–20]

In more recent literature, characteristic analysis of steady MHD flows has been applied to the study of astrophysical flows[3,4,21,22] and stationary symmetric and transonic flows.[23,24] In these papers analytical solutions of the steady MHD equations in two dimensions (2D) are obtained under various assumptions of self-similarity.

In the present article we present a detailed characteristic analysis of a stationary planar field-aligned complex MHD bow shock flow around a perfectly conducting cylinder in two space dimensions. For low values of the plasma β, switch-on shocks are possible and complex shock interaction phenomena appear[13,25] when the inflow Alfvénic Mach number is greater than one but smaller than a critical value. The numerical solution of the symmetrical steady bow shock problem in this regime was obtained by De Sterck *et al.*[13] (further referred to as DSLP98). This bow shock flow consists of two consecutive shock fronts and additional discontinuities. In DSLP98 fast shocks and tangential discontinuities were identified in the steady flow. Moreover, the presence of intermediate shocks was clearly proven and was shown to be essential to the global 2D flow structure. A thorough parameter study shows that the complex shock topology is indeed closely related to the occurrence of switch-on shocks, and a very similar topology with intermediate shocks is obtained for the axi-symmetrical field-aligned flow over a sphere in the switch-on parameter regime.[26]

In the present paper we further investigate this complicated bow shock flow using characteristic analysis of the steady MHD equations in two space dimensions (in the xy plane). A geometric view of this steady flow is presented in terms of transition lines, cusping of characteristics, limiting lines, and elliptic and hyperbolic regions in the flow. This analysis yields a clear insight into a complicated nonlinear MHD flow with interacting shocks, and the consistency of the interpretation in terms of characteristics further validates the numerical result obtained in DSLP98. Among the new results to be presented are complicated steady MHD wave structures in two space dimensions which, to the best of our

[a]Research Assistant of the Fund for Scientific Research, Flanders (Belgium). Also at the Centre for Plasma Astrophysics, Katholieke Universiteit Leuven, Belgium. Electronic mail: desterck@ucar.edu
[b]Research Associate of the Fund for Scientific Research, Flanders (Belgium).

knowledge, have not been studied before. The presence of shocks and the absence of any self-similarity assumption are new elements not present in earlier characteristic analysis of MHD flows.[3,4,21–24]

The ideal MHD equations are nonstrictly hyperbolic, as linear wave speeds may coincide. The fast and slow MHD waves are not convex,[13,27–30] which leads to the possible appearance of xt compound shocks in the solution of planar one-dimensional (1D) Riemann problems. An xt MHD compound shock is a structure composed of a sonic intermediate shock (for which the upstream or downstream plasma velocity equals the fast or the slow characteristic speed in the shock frame) with an attached rarefaction which is a simple wave.[12,14,18] Note that the term ''sonic'' is used here in a broad sense, denoting the condition that the plasma velocity equals any one of the fast, Alfvén, or slow MHD wave speeds.[24]

Intermediate shocks and compound shocks (with embedded intermediate shocks) have been found in time-dependent planar ($B_z \equiv 0$ and $v_z \equiv 0$) 1D numerical simulations.[27] The results of DSLP98 show the first clear example of intermediate MHD shocks in planar 2D simulations. In the present paper we will further investigate the planar bow shock flow of DSLP98 and look for stationary 2D compound shocks. We will compare our results with the Myong and Roe[30] study of time-dependent planar 1D MHD flows. They show analytically that most planar intermediate shocks do have viscous profiles for the case where all the dissipative parameters are equal, and that sonic intermediate shocks embedded in compound shocks are essential elements in the solution of some planar xt MHD Riemann problems. We will investigate if our analysis of a stationary planar 2D MHD flow confirms the findings which they obtained by studying time-dependent planar 1D MHD flows regarding the MHD wave features that can occur in the planar case.

The subject of the physical existence of intermediate MHD shocks has a long history and is still debated at present. For a long time it was believed that intermediate shocks are ''nonevolutionary'' and unphysical,[1,11,12,17–20] but recent numerical and theoretical results[27,29,30–40] and recent observations[25,41–43] seem to indicate that intermediate shocks can exist in the real world. However, these findings are still disputed.[44–46] The clear presence of intermediate shocks of various types in the stationary planar 2D bow shock flow of DSLP98 seems to support the recent results which state that intermediate shocks are physical. However, it is important to emphasize here that this bow shock flow belongs to the class of planar MHD flows, for which $B_z \equiv 0$ and $v_z \equiv 0$. Barmin *et al.*[44] and Falle *et al.*[45] argue that for the restricted planar system intermediate shocks are ''evolutionary'' and admissible, and can thus be expected in numerical simulation results when the simulations are restricted to planar flow, but that intermediate shocks should not occur in simulations of the full MHD system with three vector components, because they are nonevolutionary in the full MHD system and unphysical in the real world.

The question of the physical existence of intermediate and compound shocks in a nonplanar context can clearly not be addressed by our present planar simulation results. Our 2D simulation results with stationary intermediate shocks may constitute a mathematically correct and stable solution to a problem in the reduced system of planar MHD, and they confirm in 2D that intermediate shocks can indeed exist at least in planar flows, but it remains to be seen if the intermediate and compound shocks present in our 2D planar simulation results, would survive in the more general full MHD system which allows for nonplanar perturbations, given the debate on the physical existence of intermediate shocks in a nonplanar context. It is important to note that we obtain a very similar topology with intermediate shocks for the axi-symmetrical field-aligned flow over a sphere in the switch-on parameter regime.[26] Future extensions of our bow shock simulations to configurations in three space dimensions (3D) may be able to contribute to the answer to this question. In the present article, we try to understand and analyze the intricate wave structures that arise in this complicated planar 2D MHD bow shock flow.

In DSLP98, the planar complex bow shock solution was shown to contain an intermediate shock which is preceded and followed by steady rarefactions with the particular property that the normal plasma velocity is equal to a normal characteristic speed at the points where the rarefactions are attached to the shock. This is one of the basic properties of an xt compound shock.[27,28] However, the correspondence between xt compound shocks (with an attached simple wave rarefaction which is continuously expanding in time), and steady wave structures in two space dimensions (xy), is not immediately clear and does not follow trivially from the respective governing equations, although a general conceptual analogy can be expected between wave structures in the xt and the xy planes, such as demonstrated for compressible fluid dynamics.[47] Such a correspondence has also been worked out analytically for simple MHD waves in the xt and the xy planes.[18] In the present paper we will explore the correspondence between complex wave patterns in the xt and the xy planes using characteristic analysis of the steady MHD equations in two space dimensions (xy).

Our motivation is to understand the steady 2D bow shock flow of DSLP98 in terms of its characteristic structure. First, characteristic analysis will clarify the global topology of the flow in relation with elliptic and hyperbolic regions and the flow of information. Second, the detailed wave structure of some of the wave patterns present in this flow will be clarified using characteristic analysis.

This paper is organized as follows. In Sec. II we will present a concise derivation of some aspects of the characteristic theory of the MHD equations with two independent variables (time-dependent MHD in the xt plane and steady MHD in the xy plane), in preparation for the characteristic analysis of bow shock flows in the rest of the paper. This section serves to introduce the reader who is unfamiliar with the theory of characteristics to the concepts, nomenclature, and notation that will be used further on in the paper, and thus makes the paper self-contained. Moreover, our derivation of this characteristic theory, based on the Galilean invariant symmetrizable form of the conservative MHD equations with a source term[48–50] and using a matrix approach,[19,22] is new and attractive in its own right, because

it gives insight into the structure of the MHD equations as a system of Galilean invariant conservation laws with a constraint, and because in a simple, compact, and systematic way we recover all the various results that are scattered throughout the literature.[10,15–20,22]

We then apply this characteristic analysis to bow shock flows. We discuss the setup of the bow shock flows in Sec. III. The characteristic analysis of the multiple-front MHD bow shock flow of DSLP98 is quite complicated, so it is useful to gain some insight from more simple configurations first. We start out with the simple case of a traditional hydrodynamic bow shock flow in Sec. IV, followed by the characteristic analysis of a simple single-front planar MHD bow shock flow in Sec. V. In Sec. VI we discuss the characteristic structure of the complicated multiple-front planar MHD bow shock flow of DSLP98. We discuss the global topology of the flow and investigate whether or not a steady analog exists for *xt* compound shocks. We relate the results of the analysis of the flow to recent findings on stationary symmetric flows[24] and on *xt* MHD compound shocks.[27,30]

Finally, we formulate our conclusions in Sec. VII.

II. CHARACTERISTICS AND RIEMANN INVARIANTS OF MHD WITH TWO INDEPENDENT VARIABLES

It is useful for the purpose of this paper, to give a concise derivation of some aspects of the characteristic theory of the MHD equations[10,15–20,22] and an explanation of the nomenclature and notation we will use further on in this paper. We start from the general case with three vector components which gives insight in the complexity of the MHD system and the role of the $\nabla\cdot\mathbf{B}$ constraint, and then show how this complexity is reduced when we narrow our model down stepwise to the case of steady planar field-aligned homenthalpic flow.

A. The MHD equations

The equations of ideal one-fluid MHD in conservative form are given by

$$\frac{\partial}{\partial t}\begin{bmatrix}\rho\\ \rho\boldsymbol{v}\\ \mathbf{B}\\ e\end{bmatrix}+\nabla\cdot\begin{bmatrix}\rho\boldsymbol{v}\\ \rho\boldsymbol{v}\boldsymbol{v}+\boldsymbol{I}(p+\mathbf{B}\cdot\mathbf{B}/2)-\mathbf{B}\mathbf{B}\\ \boldsymbol{v}\mathbf{B}-\mathbf{B}\boldsymbol{v}\\ (e+p+\mathbf{B}\cdot\mathbf{B}/2)\,\boldsymbol{v}-(\boldsymbol{v}\cdot\mathbf{B})\mathbf{B}\end{bmatrix}=-\begin{bmatrix}0\\ \mathbf{B}\\ \boldsymbol{v}\\ \boldsymbol{v}\cdot\mathbf{B}\end{bmatrix}\nabla\cdot\mathbf{B}. \tag{1}$$

This equation has to be supplemented with the divergence free condition $\nabla\cdot\mathbf{B}=0$ as an initial condition. Here ρ and p are the plasma density and pressure, respectively, $\boldsymbol{v}$ is the plasma velocity, $\mathbf{B}$ the magnetic field, and

$$e=\frac{p}{\gamma-1}+\rho\frac{\boldsymbol{v}\cdot\boldsymbol{v}}{2}+\frac{\mathbf{B}\cdot\mathbf{B}}{2}, \tag{2}$$

is the total energy density of the plasma. $\boldsymbol{I}$ is the unity matrix. The magnetic permeability $\mu=1$ in our units. These equations describe the conservation of mass, momentum, magnetic field, and energy.

We have written Eq. (1) in an unconventional form with a source term proportional to $\nabla\cdot\mathbf{B}$ on the right hand side (RHS). This form of the equations, which reduces to the more familiar physical conservation laws when we set $\nabla\cdot\mathbf{B}=0$, can be useful for certain purposes. Godunov[48] proved in 1972 that this is the unique form of the MHD equations that is symmetrizable. It is a more general form of the MHD equations, in the sense that this form of the equations remains Galilean invariant also if $\nabla\cdot\mathbf{B}\neq0$, as will be explained in Sec. II C.

This form of the equations seems to be useful for some conservative, shock-capturing numerical schemes, as pointed out by Powell.[49] In some numerical schemes, the $\nabla\cdot\mathbf{B}=0$ constraint is only satisfied up to a discretization error. Inclusion of the RHS term is one way to assure that these small $\nabla\cdot\mathbf{B}$ errors are consistently accounted for in a numerically stable way and do not lead to accumulation of inaccuracies. An alternative would be to use a projection scheme, which applies an extra correction to the magnetic field in every time step. This correction is obtained via solution of an elliptic equation.[51,52] In DSLP98 we have used the projection method, but in the present paper we employ the source term method proposed by Powell.[49] As the reader can verify, the simulation results using these two different approaches are very similar. Only close to the stagnation point, very small differences can be observed.[43] For this bow shock simulation, we thus have a slight preference for the Powell source term method to control the $\nabla\cdot\mathbf{B}$ errors, because of two reasons. First, the source term approach consumes less computing time than the projection scheme. And second, it cures the $\nabla\cdot\mathbf{B}$ problems more in harmony with the hyperbolicity of the system, in the sense that solution of an elliptic equation contaminates the uniform upstream flow with small oscillations, whereas in theory the upstream flow should remain untouched because in the hyperbolic system signals cannot propagate upstream into a region where the flow is superfast. It may well be, however, that for some MHD flows in different parameter regimes or with different boundary conditions, the projection scheme is more appropriate.[53]

We will show that the inclusion of this RHS term is also essential for our derivation of the characteristic theory in a simple, compact, and systematic procedure using a matrix approach. Characteristic analysis based on the symmetrizable form of the conservative MHD equations gives insight into the basic structure of the MHD equations as a system of Galilean invariant conservation laws with a constraint.

B. Characteristic analysis

The basic concepts and definitions of characteristic theory can be most clearly presented for the simple scalar case. Consider a conservation law for the *scalar* quantity $u(x,t)$ which depends on two independent variables x and t

$$\frac{\partial u}{\partial t}+\frac{\partial f(u)}{\partial x}=0, \tag{3}$$

or

$$\frac{\partial u}{\partial t}+f'(u)\frac{\partial u}{\partial x}=0, \tag{4}$$

where $f(u)$ is called the flux function and the prime denotes a derivative with respect to u. If $f'(u)$ is real, then there exist curves $x(t)$ in the xt plane such that

$$\frac{dx(t)}{dt}=f'(u), \tag{5}$$

and thus

$$\frac{du(x(t),t)}{dt}=0. \tag{6}$$

Along these curves, which are called characteristics, the partial differential equation [Eq. (3)] reduces to the ordinary differential equation (6). The equation is said to be hyperbolic when $f'(u)$ is real and real characteristics exist. The scalar u is then invariant on the characteristic curve and is called a Riemann Invariant (RI). The slope of the characteristic $\lambda=f'(u)$ is called the characteristic speed. For the scalar case, the characteristics are straight lines (when f only depends on u and not directly on the independent variables). These concepts carry over to a system of conservation laws with two independent variables in the following way.

Consider a *linear* system of n coupled equations

$$\frac{\partial \boldsymbol{U}}{\partial t}+\boldsymbol{A}\cdot\frac{\partial \boldsymbol{U}}{\partial x}=0, \tag{7}$$

with $\boldsymbol{U}$ a state vector of n conserved quantities, and $\boldsymbol{A}$ a $n\times n$ constant matrix. Suppose an eigenvector decomposition of matrix $\boldsymbol{A}=\boldsymbol{R}\cdot\Lambda\cdot\boldsymbol{L}$ exists, with the columns of $\boldsymbol{R}$ being the right eigenvectors of $\boldsymbol{A}$, the rows of $\boldsymbol{L}$ being the left eigenvectors of $\boldsymbol{A}$, $\boldsymbol{R}=\boldsymbol{L}^{-1}$, and Λ being a diagonal matrix with the eigenvalues of $\boldsymbol{A}$ on the diagonal. The system is said to be hyperbolic if all the eigenvalues are real. The system can be described in terms of the characteristic variables $\boldsymbol{W}=\boldsymbol{L}\cdot\boldsymbol{U}$ as

$$\frac{\partial \boldsymbol{W}}{\partial t}+\Lambda\cdot\frac{\partial \boldsymbol{W}}{\partial x}=0. \tag{8}$$

This decouples the equations, and for every component of $\boldsymbol{W}$ we have the conservation law

$$\frac{\partial w_i}{\partial t}+\lambda_i\frac{\partial w_i}{\partial x}=0. \tag{9}$$

If the system is hyperbolic, then n characteristic curves exist in real space, defined by $dx/dt=\lambda_i$. These characteristics are straight lines, and each w_i is a RI on its associated family of characteristics.

A *nonlinear* system of n coupled equations in quasi-linear form with two independent variables is described by

$$\frac{\partial \boldsymbol{U}}{\partial t}+\boldsymbol{A}(\boldsymbol{U})\cdot\frac{\partial \boldsymbol{U}}{\partial x}=0, \tag{10}$$

where $\boldsymbol{A}(\boldsymbol{U})$ can be the Jacobian matrix of a flux function $\boldsymbol{F}$ associated with a set of conservation laws—and is hyperbolic in state $\boldsymbol{U}$ if the eigenvector decomposition of $\boldsymbol{A}(\boldsymbol{U})$ exists and all the eigenvalues of $\boldsymbol{A}(\boldsymbol{U})$ are real. The definition of the characteristic variables $\partial\boldsymbol{W}=\boldsymbol{L}(\boldsymbol{U})\cdot\partial\boldsymbol{U}$ is now only locally valid. Characteristics exist if the system is hyperbolic, and the real eigenvalues of $\boldsymbol{A}(\boldsymbol{U})$ determine the slopes of the characteristics locally. The characteristics are in general not straight lines any more, except in simple wave regions, where one family of characteristics consists of straight lines.[12,14,18] Riemann Invariants do not generally exist, but sometimes it is possible to find one or more functions χ_i of the dependent variables $\boldsymbol{U}$ such that $d\chi_i\sim\boldsymbol{L}_i\cdot d\boldsymbol{U}$, which defines χ_i as a Riemann Invariant. The mathematical interpretation of characteristic curves is that derivatives normal to the characteristic curve cannot be determined from the governing equations, because the equations only specify derivatives along the characteristic curves. The solution on a characteristic curve does not determine the solution in neighboring points not on this curve. This geometric property puts strict constraints on the posing of boundary conditions, namely, that characteristic curves cannot serve as boundaries on which boundary conditions are imposed. The physical interpretation is that weak discontinuities propagate as waves along characteristics, such that a characteristic variable is locally conserved on its corresponding characteristic (whereas Riemann Invariants are globally conserved on their characteristics). Equivalently, the wave information carried by a local characteristic variable follows a strict characteristic path and cannot escape in a direction perpendicular to the characteristic. It does not influence the solution in a neighborhood not on this characteristic.

The above analysis was placed in an xt context, and the theory of characteristics was related to concepts of propagation of physical waves in a time-dependent system. The same analysis can also be applied to steady state systems of equations, in which the time variable is not present anymore. Steady equations can also be hyperbolic, and by direct analogy we can relate the characteristic structure of steady equations to the stationary analogs of time-dependent waves, which we will call stationary waves. For instance, the concept of simple waves in MHD can be carried over from the time-dependent context (xt) to the stationary context (xy).[18] The formal analogy between the analysis of xt and xy systems of equations, both special cases of the full equations in xyt—or even $xyzt$—, can be clarified by the following considerations. In Sec. II C we will use this formal analogy to derive the characteristic properties of the xt and xy MHD equations in a unified and systematic way.

A general quasi-linear time-dependent system of n first order partial differential equations in two space dimensions is described by

$$\frac{\partial \boldsymbol{U}}{\partial t}+\boldsymbol{A}(\boldsymbol{U})\cdot\frac{\partial \boldsymbol{U}}{\partial x}+\boldsymbol{B}(\boldsymbol{U})\cdot\frac{\partial \boldsymbol{U}}{\partial y}=0, \tag{11}$$

with $\boldsymbol{U}$ a vector of dependent variables and $\boldsymbol{A}$ and $\boldsymbol{B}$ $n\times n$ matrices. This system reduces to a system with two independent variables for the case of a 1D time-dependent flow

($\partial/\partial y=0$) and for the case of a 2D steady flow ($\partial/\partial t=0$). In the first case, the last term of Eq. (11) vanishes, and the procedure which was outlined above can be used to study the characteristic structure of the equations. In the second case, the first term of Eq. (11) vanishes, and one can examine the characteristic properties of the equation

$$\frac{\partial \boldsymbol{U}}{\partial x}+\boldsymbol{A}^{-1}\cdot\boldsymbol{B}\cdot\frac{\partial \boldsymbol{U}}{\partial y}=0, \tag{12}$$

leading to characteristic analysis in the xy plane. The eigenvalues and left eigenvectors of the matrix $\boldsymbol{C}\equiv\boldsymbol{A}^{-1}\cdot\boldsymbol{B}$ again determine the type of the system, the characteristic directions in the xy plane, and the Riemann Invariants.

C. Characteristic analysis of the MHD equations with two independent variables

In this section, the above sketched general framework is applied to the MHD equations and a derivation is presented of some aspects of the characteristic theory of the MHD equations.[10,15–20,22] We will analyze the symmetrizable form of the equations [Eq. (1)], and will not use the condition $\nabla\cdot\mathbf{B}=0$, unless where necessary and stated. In this way we will be able to see how the characteristic structure of the MHD equations is independent of the $\nabla\cdot\mathbf{B}$ constraint, and when this constraint becomes important.

For simplicity, we consider a perfect gas, such that the sound speed is given by

$$c=\sqrt{\gamma p/\rho}, \tag{13}$$

and the entropy is given by

$$s=p/\rho^{\gamma}. \tag{14}$$

The hydrodynamic stagnation enthalpy is defined as

$$h_s\equiv\frac{\gamma}{\gamma-1}\frac{p}{\rho}+\frac{1}{2}v^2, \tag{15}$$

and will play a role in the analysis of field-aligned MHD flow.

Equation (1) can be written in the quasi-linear form of Eq. (11) with $\boldsymbol{U}=(\rho,v_x,v_y,v_z,B_x,B_y,B_z,p)$ the vector of so-called ''primitive'' variables [as opposed to the vector of ''conserved variables'' $(\rho,\rho v_x,\rho v_y,\rho v_z,B_x,B_y,B_z,e)$ used in Eq. (1)], and matrices

$$\boldsymbol{A}=\begin{bmatrix} v_x & \rho & 0 & 0 & 0 & 0 & 0 & 0\\ 0 & v_x & 0 & 0 & 0 & B_y/\rho & B_z/\rho & 1/\rho\\ 0 & 0 & v_x & 0 & 0 & -B_x/\rho & 0 & 0\\ 0 & 0 & 0 & v_x & 0 & 0 & -B_x/\rho & 0\\ 0 & 0 & 0 & 0 & v_x & 0 & 0 & 0\\ 0 & B_y & -B_x & 0 & 0 & v_x & 0 & 0\\ 0 & B_z & 0 & -B_x & 0 & 0 & v_x & 0\\ 0 & c^2\rho & 0 & 0 & 0 & 0 & 0 & v_x \end{bmatrix} \tag{16}$$

and

$$\boldsymbol{B}=\begin{bmatrix} v_y & 0 & \rho & 0 & 0 & 0 & 0 & 0\\ 0 & v_y & 0 & 0 & -B_y/\rho & 0 & 0 & 0\\ 0 & 0 & v_y & 0 & B_x/\rho & 0 & B_z/\rho & 1/\rho\\ 0 & 0 & 0 & v_y & 0 & 0 & -B_y/\rho & 0\\ 0 & -B_y & B_x & 0 & v_y & 0 & 0 & 0\\ 0 & 0 & 0 & 0 & 0 & v_y & 0 & 0\\ 0 & 0 & B_z & -B_y & 0 & 0 & v_y & 0\\ 0 & 0 & c^2\rho & 0 & 0 & 0 & 0 & v_y \end{bmatrix}. \tag{17}$$

The xt characteristic analysis yields the following results. The eigenvalues of matrix $\boldsymbol{A}$ are

$$\lambda_{1,2}=v_x\pm c_f,\quad \lambda_{3,4}=v_x\pm c_A,\quad \lambda_{5,6}=v_x\pm c_s,\quad \lambda_{7,8}=v_x. \tag{18}$$

These eigenvalues are always real, meaning that the system is always hyperbolic, and the eigenvalues thus determine the characteristic directions in the xt plane. The left eigenvectors

$$\boldsymbol{L}_7=(-c^2,0,0,0,0,0,0,1)\quad\text{and}\quad \boldsymbol{L}_8=(0,0,0,0,1,0,0,0), \tag{19}$$

can be used to derive the Riemann Invariants

$$\chi_7=s\quad\text{and}\quad \chi_8=B_x. \tag{20}$$

For instance, the condition that $\boldsymbol{L}_7\cdot d\boldsymbol{U}=0$ in the direction of the characteristic with slope v_x, can be written as $\boldsymbol{L}_7\cdot(d\rho,dv_x,dv_y,dv_z,dB_x,dB_y,dB_z,dp)=-c^2d\rho+dp=0$. This leads to $ds=0$, because it follows from Eq. (14) that $ds=dp/\rho^{\gamma}-\gamma p/\rho^{\gamma+1}d\rho=(-c^2d\rho+dp)/\rho^{\gamma}$. This means that the entropy s is a RI. Making use of $\nabla\cdot\mathbf{B}=0$, it follows from Eq. (1) that B_x has to be constant in x and t, such that B_x is a global RI (with a constant value in the whole xt domain), and can thus be eliminated from the xt equations, resulting in the more common description of 1D time-dependent MHD with seven dependent variables. Here we can also clarify why we had to include the RHS term in Eq. (1): Omission of this term results in an eigenvalue $\lambda_8=0$,[49] which is not a Galilean invariant property, because a change in reference frame would change v_x and thus all the wave speeds accordingly, except λ_8, which would remain zero also in the new reference frame. This zero eigenvalue makes matrix $\boldsymbol{A}$ singular, such that the general procedure outlined above to derive the xy characteristics, which uses $\boldsymbol{A}^{-1}$, would fail.

For steady state solutions the xy characteristic analysis yields the following results. In the stationary case, the governing equations are not always fully hyperbolic. If some eigenvalue of matrix $\boldsymbol{C}=\boldsymbol{A}^{-1}\cdot\boldsymbol{B}$ is not real, then its associated characteristic does not exist. It is hard to find closed expressions for the eigenvalues of matrix $\boldsymbol{C}=\boldsymbol{A}^{-1}\cdot\boldsymbol{B}$, but using software for symbolical calculation, we can easily factorize the condition $\det(\boldsymbol{C}-\lambda\boldsymbol{I})=0$ in terms of the variable

$$v_{\perp}^2=\frac{(-v_y+v_x\lambda)^2}{1+\lambda^2}, \tag{21}$$

which represents the square of the velocity component perpendicular to the characteristic, as the direction of the characteristic is given by $dy/dx=\lambda$. This factorization leads to the following roots:

$$v_{\perp 1}^2=c_{f\perp}^2, \quad v_{\perp 2}^2=c_{A\perp}^2, \quad v_{\perp 3}^2=c_{s\perp}^2, \quad v_{\perp 4}^2=0, \tag{22}$$

where $c_{f\perp}$, $c_{A\perp}$, and $c_{s\perp}$ are the fast magnetosonic, Alfvén, and slow magnetosonic velocities in the direction perpendicular to the characteristic.[18,22] For every condition (22), if real λs can be found which satisfy the condition, then the associated characteristics exist and we say that the associated characteristic fields are hyperbolic.

The physical interpretation of these conditions is clear: If they exist, then the xy characteristics are curves from which no wave information carried by the associated characteristic variable can escape in a direction perpendicular to the characteristic. For instance, the wave with wave speed $v_\perp - c_{f\perp}$ perpendicular to the characteristic cannot transport information in this perpendicular direction when $v_\perp = c_{f\perp}$. This defines the steady xy characteristics as curves on which the perpendicular plasma speed equals a perpendicular wave speed. We say that the flow is sonic in the direction perpendicular to the characteristic.

The equation for $v_{\perp 4}$ always has two real solutions, $\lambda_{7,8}=v_y/v_x$, meaning that the streamlines are twofold degenerate characteristics. The associated left eigenvectors are

$$\boldsymbol{L}_7=(-c^2,0,0,0,0,0,0,1)$$

and (23)

$$\boldsymbol{L}_8=(0,B_y/v_x,-B_x/v_x,0,-v_y/v_x,1,0,0),$$

and can be used to derive the Riemann Invariants

$$\chi_7=s \quad \text{and} \quad \chi_8=v_xB_y-v_yB_x=E_z, \tag{24}$$

with E_z the z component of the electric field. Making use of $\nabla\cdot\mathbf{B}=0$, it follows from Eq. (1) that Riemann Invariant $\chi_8=E_z$ is a global invariant, as with $\nabla\cdot\mathbf{B}=0$ the evolution equation of the magnetic field reduces to the classical form of the induction equation $\partial\mathbf{B}/\partial t=-\nabla\times\mathbf{E}$. Then $\partial\mathbf{B}/\partial t=-\nabla\times\mathbf{E}=0$ leads to $\partial E_z/\partial x=\partial E_z/\partial y=0$. E_z can thus be eliminated from the equations. The entropy is conserved on a streamline in continuous flow. However, it follows from the MHD Rankine–Hugoniot (RH) jump conditions[1,11,12] that the entropy is discontinuous when a streamline crosses a shock.

The equation for $v_{\perp 2}$ always has two real solutions as well, $\lambda_{3,4}=(B_y\pm\sqrt{\rho}v_y)/(B_x\pm\sqrt{\rho}v_x)$.

The equations for $v_{\perp 1}$ and $v_{\perp 3}$ are much more complicated. Depending on the parameters, the equation for $v_{\perp 1}$ can have no solution or two solutions for λ. The equation for $v_{\perp 3}$ can have zero, two, or four real solutions for λ, with the total number of real solutions for the two equations not exceeding four. The slow and fast magnetosonic characteristic fields can thus be hyperbolic or elliptic depending on the parameters, and no simple formulas can be found as criteria for hyperbolicity. Graphical methods can be used to determine the hyperbolic and elliptic regions of the equations.[15–20,22]

In the case of planar MHD ($B_z\equiv 0$ and $v_z\equiv 0$), the Alfvén waves disappear, meaning that the families of characteristics corresponding to characteristic speeds λ_3 and λ_4 drop out, both in the xt and in the xy case. The other characteristic families remain unchanged.

For steady MHD in two space dimensions, if the components of the magnetic field in the xy plane are aligned to the xy components of the flow velocity somewhere in the xy domain, then $E_z=0$ at that location. It then follows from the analysis given above, that the magnetic field in the xy plane has to be aligned to the flow everywhere, as E_z is a global invariant and thus vanishes everywhere. It can be proved using the MHD RH relations, that this property is also conserved at shocks (as the tangential electric field is conserved at a shock). These properties establish the concept of steady field-aligned MHD flow.

It is interesting to note that the characteristic structure of the MHD equations is independent of the constraint $\nabla\cdot\mathbf{B}=0$. The characteristic structure derived from the symmetrizable form of the equations [Eq. (1)] is consistent and complete, without the need to impose the $\nabla\cdot\mathbf{B}=0$ constraint. The concept of field-aligned flow however requires that $\nabla\cdot\mathbf{B}=0$, because only then E_z is a global invariant.

D. Characteristic analysis of steady planar field-aligned MHD

The bow shock flows which we will analyze further on in this paper, belong to the class of steady planar field-aligned MHD. Therefore, we will now show how the above derived general results on characteristic analysis of the MHD equations simplify for this special case.[15,16,19,21,22]

We introduce the variable α in Eq. (1) with $\partial/\partial t=0$ by taking $\mathbf{B}=\alpha\boldsymbol{v}$. The steady MHD equations for planar field-aligned flow reduce then to a 5×5 system with $\boldsymbol{U}=(\rho,v_x,v_y,\alpha,p)$, and matrices

$$\boldsymbol{A}=\begin{bmatrix} v_x & \rho & 0 & 0 & 0 \\ 0 & v_x & \alpha^2 v_y/\rho & \alpha v_y^2/\rho & 1/\rho \\ 0 & 0 & (1-\alpha^2/\rho)v_x & -\alpha v_x v_y/\rho & 0 \\ 0 & \alpha & 0 & v_x & 0 \\ 0 & c^2\rho & 0 & 0 & v_x \end{bmatrix} \tag{25}$$

and

$$\boldsymbol{B}=\begin{bmatrix} v_y & 0 & \rho & 0 & 0 \\ 0 & (1-\alpha^2/\rho)v_y & 0 & -\alpha v_x v_y/\rho & 0 \\ 0 & \alpha^2 v_x/\rho & v_y & \alpha v_x^2/\rho & 1/\rho \\ 0 & 0 & \alpha & v_y & 0 \\ 0 & 0 & c^2\rho & 0 & v_y \end{bmatrix}. \tag{26}$$

Note that, consistent with our observations at the end of Sec. II C, the fourth row of the equations now automatically leads to $\nabla\cdot(\boldsymbol{\alpha v})=\nabla\cdot\mathbf{B}=0$, although we have only explicitly imposed that $\alpha\boldsymbol{v}=\mathbf{B}$, and not that $\nabla\cdot\mathbf{B}=0$.

Analysis of the characteristic properties of this 5×5 system yields the following results. The characteristic condition $\det(\boldsymbol{C}-\lambda\boldsymbol{I})=0$ can again be factorized in terms of the variable $v_\perp^2$. This factorization leads to the following roots:

$$v_{\perp 1}^2=c^2(1-\alpha^2/\rho)+v^2\alpha^2/\rho \quad \text{and} \quad v_{\perp 2}^3=0. \tag{27}$$

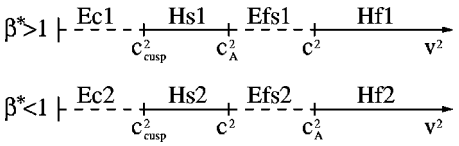

FIG. 1. Elliptic and hyperbolic regions in parameter space for steady planar field-aligned MHD. The top line corresponds to $\beta^*>1$, and shows, as v^2 decreases, a division in a fast hyperbolic region (Hf1), an elliptic region between the fast and the slow hyperbolic regions (Efs1), a slow hyperbolic region (Hs1), and an elliptic region below the cusp speed (Ec1). The bottom line shows a similar division for $\beta^*<1$. For $\beta^*=1$, $c^2=c_A^2$.

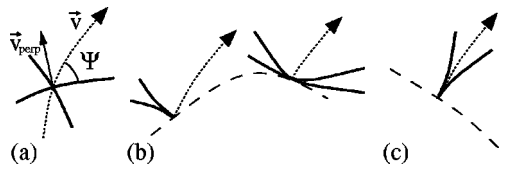

FIG. 2. Streamlines (dotted), slow or fast characteristics (thick), and transition lines between hyperbolic and elliptic regions (dashed), for steady planar field-aligned MHD. (a) The two families of characteristics (thick) both make an angle ψ with the streamline. (b) At transition lines where the plasma velocity equals the sound speed or the Alfvén speed, the characteristics become perpendicular to the streamline. When the streamline is perpendicular to the transition line, the characteristics will be tangent to the transition line. (c) At transition lines where the plasma velocity equals the cusp speed, the characteristics cusp and are tangent to the streamline.

The equation for $v_{\perp 2}$ always has three real solutions, $\lambda_{3,4,5}=v_y/v_x$, meaning that the streamlines are threefold degenerate characteristics. The corresponding left eigenvectors are

$$\boldsymbol{L}_3=(-c^2,0,0,0,1), \quad \boldsymbol{L}_4=(-\alpha/\rho,0,0,1,0),$$
$$\text{and} \tag{28}$$
$$\boldsymbol{L}_5=(c^2/(\rho v_y),v_x/v_y,1,0,0),$$

and can be used to derive the Riemann Invariants

$$\chi_3=s, \quad \chi_4=\rho/\alpha, \quad \text{and} \quad \chi_5=h_s. \tag{29}$$

The entropy, ρ/α, and the stagnation enthalpy are thus conserved on a streamline in continuous flow. It follows from the MHD Rankine–Hugoniot (RH) jump conditions,[1,11,12] that the entropy is discontinuous when a streamline crosses a shock. However, the stagnation enthalpy and ρ/α are conserved over a shock. The invariance of these three quantities along streamlines can also be derived by direct manipulation of the conservation laws of Eq. (1). For instance, using $\nabla\cdot\mathbf{B}=0$ and $\mathbf{B}=\alpha\boldsymbol{v}$, one can see that $\nabla\cdot(\rho\boldsymbol{v})=\nabla\cdot(\rho/\alpha\alpha\boldsymbol{v})=\alpha\boldsymbol{v}\cdot\nabla(\rho/\alpha)+\rho/\alpha\nabla\cdot(\alpha\boldsymbol{v})=\alpha\boldsymbol{v}\cdot\nabla(\rho/\alpha)$. Because $\nabla\cdot(\rho\boldsymbol{v})=0$ in a steady state, this leads to $\boldsymbol{v}\cdot\nabla(\rho/\alpha)=0$, which means that ρ/α is conserved on a streamline.

The solutions of the equation for $v_{\perp 1}$ are

$$\lambda_{1,2}=\frac{\rho v_x v_y \pm \sqrt{(v^2-c^2)(\alpha^2-\rho)(c^2(\alpha^2-\rho)-v^2\alpha^2)}}{\rho(c^2-v_x^2)-\alpha^2(c^2-v^2)}. \tag{30}$$

If the factor under the square root sign is positive, then these eigenvalues are real, and the equations are hyperbolic.[15–22] This factor changes sign three times, viz. when the square of the velocity equals

$$v^2=c_A^2, \quad v^2=c^2, \quad \text{and} \quad v^2=c_{\text{cusp}}^2. \tag{31}$$

The cusp velocity is defined as $c_{\text{cusp}}^2=(c^2c_A^2)/(c^2+c_A^2)$ and is the velocity of the slow wave cusp in the MHD Friedrichs diagram.[16,17] Note that we define c_A as the Alfvén speed in the direction of the magnetic field in the case of field-aligned flow. This leads to a division of the parameter space into elliptic and hyperbolic regions, as depicted in Fig. 1, for high and low β^*, where the parameter β^* is defined as $\beta^*=p/(B^2/\gamma)=c^2/c_A^2$.

In Fig. 2(a) the local geometry of streamlines and xy characteristics is sketched for the case of planar steady field-aligned MHD in hyperbolic regions. The streamline is a threefold degenerate characteristic, and there are two additional families of characteristics (generalized Mach lines[10,14]) which make equal angles ψ with the streamline. These characteristics can be of the slow or fast type, depending on which hyperbolic regime the parameters are in (Hf or Hs of Fig. 1). Division of the expression for $v_{\perp 1}^2$ in Eq. (27) by v^2 leads to the following interesting formula for the angle ψ between the streamline and the characteristic [Fig. 2(a)]:

$$\sin^2\psi=\frac{v_\perp^2}{v^2}=\frac{M^2+M_A^2-1}{M^2M_A^2}. \tag{32}$$

The sonic and Alfvénic Mach numbers are defined as $M=v/c$ and $M_A=v/c_A$. The flow is hyperbolic when $0\leqslant(M^2+M_A^2-1)/(M^2M_A^2)\leqslant 1$. For $v^2=c_A^2$ $(M_A^2=1)$ or $v^2=c^2$ $(M^2=1)$, $v_\perp^2$ equals v^2 and $\psi=90°$, meaning that at such transition lines between elliptic and hyperbolic regions, the characteristics will be perpendicular to the streamlines, as is shown in Fig. 2(b). At transition lines of these types, characteristics can thus only be parallel to these lines when the streamline is perpendicular to the transition line. For $v^2=c_{\text{cusp}}^2$, $v_\perp^2$ equals zero and $\psi=0°$, meaning that at this type of transition line between elliptic and hyperbolic regions, the characteristics cusp parallel to the streamlines,[3,21] as is shown in Fig. 2(c).

In some cases further simplifications can be made. If the stagnation enthalpy is the same on every streamline (this is called homenthalpic flow), then p can be eliminated from the equations, resulting in a 4×4 system with $\boldsymbol{U}=(\rho,v_x,v_y,\alpha)$. In this case λ_5 and χ_5 drop out, but the rest of the analysis remains the same. Similarly, steady planar hydrodynamics in 2D results in a 4×4 system with $\boldsymbol{U}=(\rho,v_x,v_y,p)$. The results for this special case of vanishing magnetic field are recovered by putting $\alpha=0$, in which case λ_4 and χ_4 drop out.

A summary of the results on characteristic analysis of the MHD equations with two independent variables is given in Table I. We are now ready to apply this characteristic theory to the analysis of numerically obtained bow shock flow solutions.

As a final remark, we can note that the concepts of characteristic analysis can be extended to systems with three and four independent variables.[10,54] The matter becomes quite more complicated, and necessitates the introduction of concepts like characteristic rays, surfaces, and cones. For the

TABLE I. Overview of some characteristic properties of the MHD equations, for full (8×8) MHD [$\boldsymbol{U}=(\rho,v_x,v_y,v_z,B_x,B_y,B_z,p)$] in the xt and the xy planes, and for steady planar field-aligned MHD [5×5, $\boldsymbol{U}=(\rho,v_x,v_y,\alpha,p)$] in the xy plane. The first column labels the characteristic fields as in the text. The second column gives the characteristic directions λ or the condition on $v_\perp$ for every characteristic field. The third column gives the Riemann Invariants. The fourth column gives the multiplicity of the real eigenvalues, and thus indicates if the corresponding characteristic fields are hyperbolic or elliptic.

Characteristic field	λ or $v_\perp$	RI	Multiplicity
MHD (8×8), xt			
1,2	$\lambda=v_x\pm c_f$		2
3,4	$\lambda=v_x\pm c_A$		2
5,6	$\lambda=v_x\pm c_s$		2
7,8	$\lambda=v_x$	$s,\ B_x$	2
MHD (8×8), xy			
1,2	$v_\perp^2=c_{f\perp}^2$		0—2
3,4	$v_\perp^2=c_{A\perp}^2$		2
5,6,1,2	$v_\perp^2=c_{s\perp}^2$		0—2—4
7,8	$v_\perp^2=0$	$s,\ v_xB_y-v_yB_x$	2
planar $\mathbf{B}\|\boldsymbol{v}$ **MHD** (5×5), xy			
1,2	$v_\perp^2=c^2(1-\alpha^2/\rho)+v^2\alpha^2/\rho$		0—2
3,4,5	$v_\perp^3=0$	$s,\ \rho/\alpha,\ h_s$	3

purpose of this paper, it is however not necessary to consider systems with more than two independent variables.

III. BOW SHOCK FLOWS OVER A PERFECTLY CONDUCTING PLATE WITH A SEMICYLINDRICAL BUMP

In the following sections, we will discuss symmetrical bow shock flows generated when a uniform field-aligned flow over a perfectly conducting plate is obstructed by a semicylindrical perfectly conducting bump or corner (Fig. 3). For sufficiently large inflow velocities a steady state bow shock is formed. The flow can be studied in the left quadrant bounded on the right by a vertical line through the center of the cylinder, at which the flow is superfast.

The bow shock flows are obtained numerically by solving the time-dependent ideal MHD equations Eq. (1) on a stretched polar-like structured grid using a finite volume method which is second order accurate in space and time.

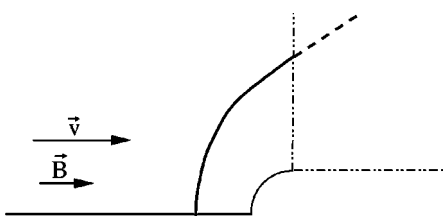

FIG. 3. Sketch of the bow shock flow configuration under study. A uniform field-aligned flow over a perfectly conducting plate comes in from the left and encounters a semicylindrical perfectly conducting rigid bump or corner. A steady state bow shock is formed. The flow can be studied in the left quadrant bounded on the right by a vertical line through the center of the cylinder, at which the flow is supersonic.

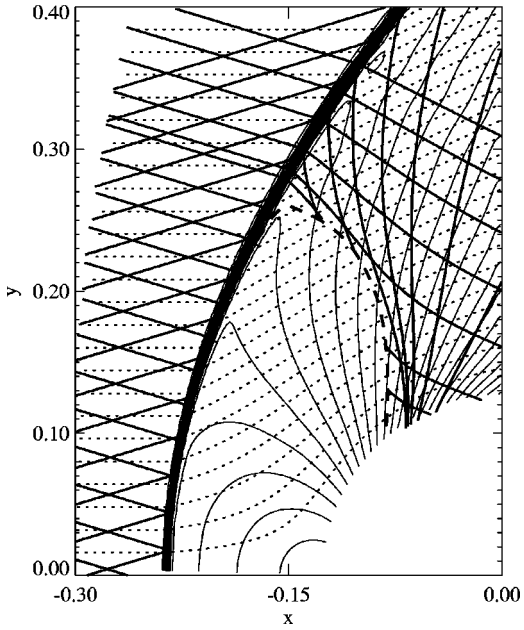

FIG. 4. Bow shock flow for the hydrodynamic case ($v_x=2, B_x=0$). The shock is clearly seen where the density contours (thin solid lines) are piling up. The streamlines (dotted) are double characteristics with s and h_s as associated Riemann Invariants. The thick solid lines are the two families of hydrodynamic characteristics (Mach lines) making equal angles with the streamlines. The thick dashed transition line is the $M=1$ contour, separating the subsonic elliptic region close to the cylinder from the rest of the flow, which is supersonic and thus hyperbolic. The Mach lines are perpendicular to the streamlines at the transition line.

We use the Lax–Friedrichs numerical flux function[44,52] and Powell's source term technique[49] to keep the $\nabla\cdot\mathbf{B}$ constraint satisfied. The steady state solution is obtained by means of a time marching procedure (see DSLP98 for details and references). The numerical code used for these bow shock simulations was previously used for resistive MHD simulations of interacting hot filaments in a tokamak[9] and for the simulation of explosive events in the solar atmosphere.[55,56]

In the following sections, we choose the values of the incoming flow variables as follows: $\rho=1, p=0.2, v_y=0, B_y=0$. The values of v_x and B_x will be varied. The bow shock flows considered in this paper are planar flows, which means that $B_z\equiv 0$ and $v_z\equiv 0$ in the whole simulation domain. The flow solution scales with the radius of the cylinder which can thus be chosen arbitrarily. We choose $r_{\text{cyl}}=0.125$ and we take $\gamma=\frac{5}{3}$ for all simulations.

IV. HYDRODYNAMIC BOW SHOCK

In Fig. 4 we show the simulation result of a hydrodynamic bow shock with $v_x=2$ and $B_x=0$ for the incoming flow. The shock is clearly seen where the density contours (thin solid lines) are piling up. The streamlines (dotted) are double characteristics with s and h_s as the corresponding Riemann Invariants along these characteristics. The thick solid lines are the two families of hydrodynamic characteristics (Mach lines[14]) making equal angles ψ with the streamlines. The thick dashed transition line is the $M=1$ contour, separating the subsonic elliptic region close to the cylinder from the rest of the flow, which is supersonic and thus hy-

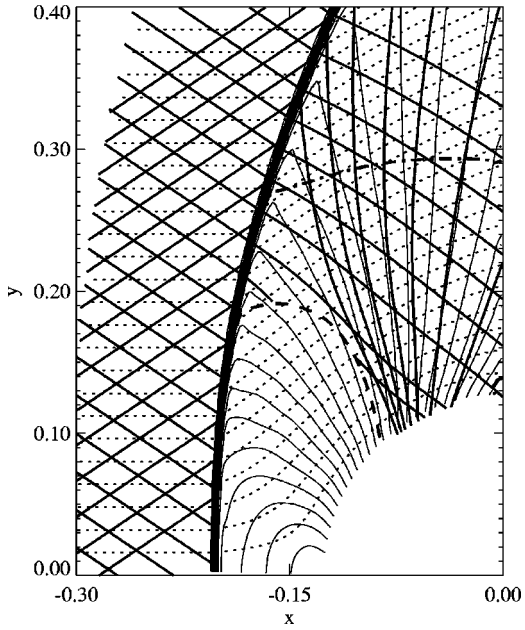

FIG. 5. Bow shock flow for the fast MHD case ($v_x=2, B_x=1$). The bow shock has the traditional single-front topology, and the characteristic properties of the flow are very similar to the hydrodynamic case. Density contours (thin solid lines) pile up in the shock. The streamlines (which are also magnetic field lines) are dotted. The thick solid lines are two families of fast characteristics making equal angles with the streamlines. The thick dashed transition line is the $M=1$ contour, separating the subsonic elliptic region close to the cylinder (Efs1) from the rest of the flow, which is supersonic and thus hyperbolic (Hf2 and Hf1). The fast characteristics are perpendicular to the streamlines at the transition line. The thick dash-dotted line is the $\beta^*=1$ contour.

perbolic. The Mach lines are perpendicular to the streamlines at the transition line, corresponding to Fig. 2(b). Limiting characteristics[14,24] (or limiting lines) are the convex hulls of characteristics which appear when characteristics of one family start to pile up and develop those convex hulls. Limiting characteristics cannot exist in real flows, unless they are perpendicular to the streamlines. They are generally avoided through the appearance of shocks,[14,24] because at the location of the limiting characteristic the solution would be multivalued. In the bow shock flow of Fig. 4 it is indeed seen that limiting lines are not present, but that shocks bring the flow from the upstream supersonic state to a downstream elliptic (close to the cylinder) or hyperbolic (further away from the cylinder) state.[24]

V. SINGLE-FRONT MHD BOW SHOCK

In Fig. 5 we show the simulation result of a fast MHD bow shock with $v_x=2$ and $B_x=1$ for the incoming flow. The inflow plasma β is low, but these inflow parameters do not allow for switch-on shocks (see DSLP98), so that we get a simple traditional single-front MHD bow shock. The characteristic properties of the flow are very similar to the hydrodynamic case. Density contours (thin solid lines) pile up in the shock. The streamlines (which are also magnetic field lines) are dotted. The thick solid lines are two families of fast characteristics making equal angles with the streamlines. The angle ψ is a little larger, such that the bow shock and the characteristics are opened up a little compared to the hydrodynamic case. The influence of the magnetic field on this angle is clear: The angle will always be larger than the corresponding hydrodynamic angle ($B_x=0$), as

$$\sin^2\psi_{\mathrm{MHD}}=\frac{M^2+M_A^2-1}{M^2M_A^2}\geqslant\sin^2\psi_{\mathrm{HD}}=\frac{1}{M^2}, \tag{33}$$

for supersonic flow ($M^2\geqslant 1$).

We can determine the types of the hyperbolic and elliptic regions in the flow according to the classification given in Fig. 1. The parameter β^* is smaller than one upstream, and greater than one downstream from the shock, except far away from the cylinder (the thick dash–dotted line is the $\beta^*=1$ contour). The thick dashed transition line is the $M=1$ contour, separating the subsonic elliptic region close to the cylinder (Efs1) from the rest of the flow, which is supersonic and thus hyperbolic (Hf2 upstream from the shock and downstream far from the cylinder, and Hf1 downstream and closer to the cylinder). The fast characteristics are perpendicular to the streamlines at the transition line, corresponding to Fig. 2(b). The comments regarding limiting characteristics that were given in the hydrodynamic case, can be repeated for this fast MHD bow shock flow.

VI. MULTIPLE-FRONT MHD BOW SHOCK

In Fig. 6(a) we show the simulation result of the MHD bow shock flow with $v_x=1.5$ and $B_x=1$ for the incoming flow. The inflow plasma β is low ($\beta=0.4$), and the inflow parameters allow for switch-on shocks, so that we get a complex interacting multiple-front MHD bow shock flow. We refer the reader to DSLP98 for a detailed discussion of this complicated flow. The angle ψ in the upstream part is larger than in the single-front case of Sec. V. The bow shock is opened up even more and a ''dimple'' appears in the shock front near the conducting plate, where the front is now curved convex outward from the cylinder. A second shock front is seen to have separated from the leading shock front. Additional discontinuities can be seen between these two shock fronts.

These complex shock interaction phenomena lead to a flow which is quite a bit more complicated in terms of characteristic analysis. The dotted lines again indicate the streamlines, and the thick solid lines indicate the two families of characteristics which are of the slow or fast type depending on the location in the flow. Several separate elliptic regions can be seen.

These shock interaction effects are described in great detail in DSLP98. Here we will just identify the different shock fronts in terms of their shock type[1,11,13] and clarify the global topology of the flow. Figure 6(b) shows a sketch of the shock topology, with lettering labels that will be used to refer to shock parts. The possible plasma states upstream and downstream from an MHD shock are traditionally labeled with the numbers 1 to 4, with state 1 a super-fast state, state 2 sub-fast but super-Alfvénic, state 3 sub-Alfvénic but super-slow, and state 4 sub-slow.[1,11,13] In the leading front, shock AB is a 1–2 fast shock, BCD is 1–3 intermediate, DE is 1–2 fast, and EF is 1–4 hydrodynamic. The second front

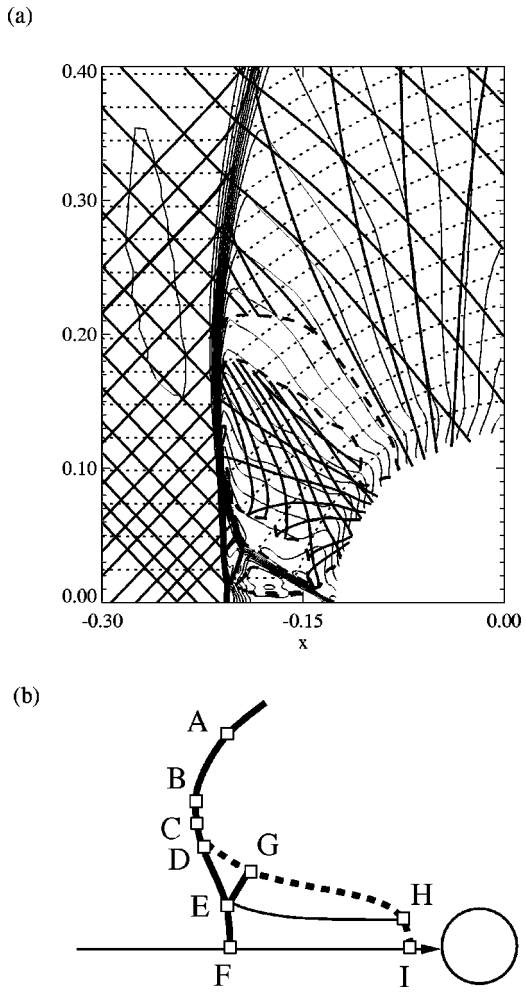

FIG. 6. (a) Interacting bow shock flow for the complex MHD case ($v_x=1.5$, $B_x=1$). A ''dimple'' appears in the leading shock front near the conducting plate, and a second shock front is seen to have separated from the leading shock front. Additional discontinuities can be seen between the two shock fronts. Density contours (thin solid lines) pile up in the shocks. The streamlines (which are also magnetic field lines) are dotted. The thick solid lines are two families of fast characteristics making equal angles with the streamlines. Several elliptic and hyperbolic regions are present. (b) Shock topology of the interacting bow shock solution.

$DGHI$ is 2–4 intermediate (almost 2=3–4 slow switch-off). EG is a 1=2–3=4 intermediate shock which is sonic both upstream and downstream. EH is a tangential discontinuity, and tangential discontinuities also stretch out from points D, G, and H, along the streamlines towards infinity.

A. Elliptic and hyperbolic regions

In Fig. 7 we analyze the hyperbolicity of the flow. The thick solid line is the $\beta^*=1$ contour. The $M=1$ contour (thick dashed), the $M_A=1$ contour (thick dotted), and the $M_{\text{cusp}}=1$ contour (thick dash–dotted), are the transition lines between elliptic and hyperbolic regions. We can label the regions according to the classification of Fig. 1. The incoming flow is hyperbolic of the type Hf2. Downstream of the leading and the second shock fronts, and starting from above, the flow is first hyperbolic of the type Hf2, and becoming hyperbolic of the type Hf1 as the $\beta^*=1$ contour is crossed. Crossing the $M=1$ contour brings us into an elliptic region

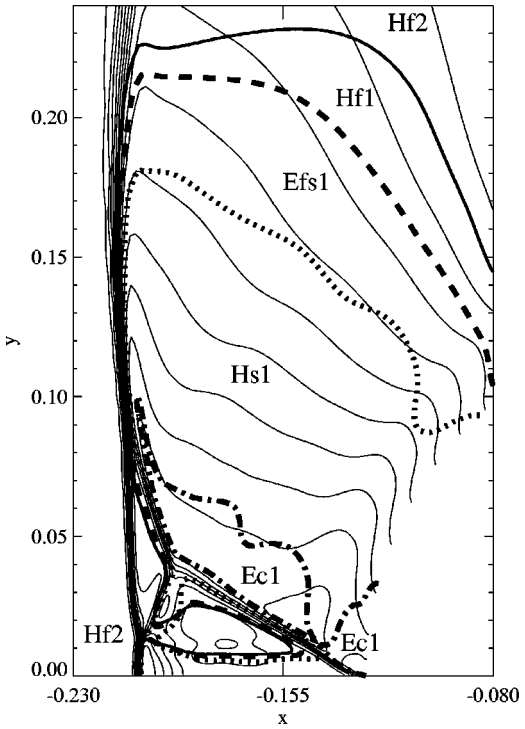

FIG. 7. Elliptic and hyperbolic regions in the bow shock flow. Density contours (thin solid lines) pile up in the shocks. The $\beta^*=1$ contour (thick solid), the $M=1$ contour (thick dashed), the $M_A=1$ contour (thick dotted), and the $M_{\text{cusp}}=1$ contour (thick dash–dotted) separate the different regions.

of type Efs1, followed by a hyperbolic region of type Hs1 when the $M_A=1$ contour is crossed. In Fig. 6(a) we can see that the characteristics are perpendicular to the streamlines at these transition lines. Further down, we reach the elliptic region of type Ec1 as the $M_{\text{cusp}}=1$ contour is crossed. At this transition line, the characteristics show the expected cusping behavior of Fig. 2(c), as can be seen in Fig. 6(a).

In Fig. 8 we show a more detailed plot of the interaction region near the conducting plate. The incoming flow is Hf2, and it remains Hf2 through the fast shock DE. Shock EG brings the flow into a Hs1 region a, as we cross the $\beta^*=1, M=1$, and $M_A=1$ contours simultaneously. From re-

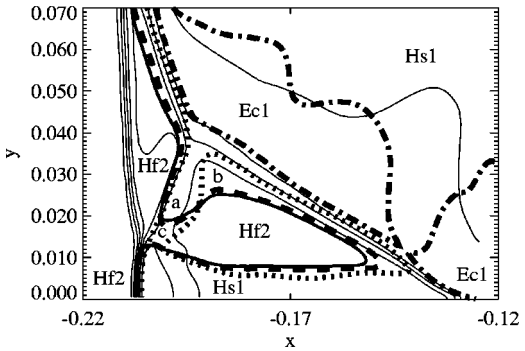

FIG. 8. Elliptic and hyperbolic regions in the bow shock flow near the conducting plate. Density contours (thin solid lines) pile up in the shocks. The $\beta^*=1$ contour (thick solid), the $M=1$ contour (thick dashed), the $M_A=1$ contour (thick dotted), and the $M_{\text{cusp}}=1$ contour (thick dash–dotted) separate the different regions. Region a is Hs1, region b is Efs1, and region c is Efs2.

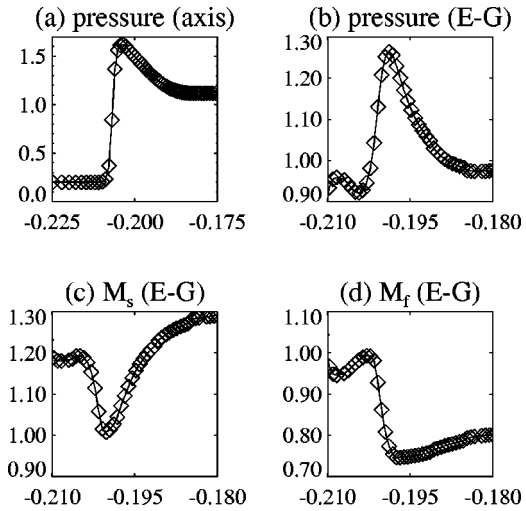

FIG. 9. (a) Pressure along the conducting plate near the leading shock. The shock is followed by a rarefaction. (b)–(d) Pressure, slow Mach number, and fast Mach number in the direction along the perpendicular cut through shock EG which is shown in Fig. 13 (thin dotted line). The shock is preceded and followed by rarefactions, which are sonic where they are attached to the shock.

gion a crossing the $M_A=1$ contour leads us to a Efs1 region b, and crossing the $\beta^*=1$ and $M=1$ contours leads to a Efs2 region c. Near the conducting plate at the bottom, shock EF brings the flow into a Hs1 region, as the $\beta^*=1, M=1$, and $M_A=1$ contours are crossed simultaneously. Enclosed between regions c, b, and the Hs1 region at the bottom, we find a Hf2 region.

As could be expected, we do not encounter limiting lines in this flow, but instead we find shocks. Shock transitions exist between two hyperbolic regions (for example, from Hf2 to Hf2 through shock DE, and from Hf2 to Hs1 through shocks EG, EF, and BD), between a hyperbolic and an elliptic region (for example, from Hf2 to Efs1 above point B ($M_A=1$ downstream of point B), and from Hf2 to Ec1 through shock DG), and apparently also between elliptic regions of different types [from region b (Efs1) to Ec1 through shock GH], although we have to remain careful with our conclusions as the numerical resolution is not very high in this small region. This last type of shock transition from elliptic to elliptic may be surprising at first sight, but a similar theoretical result has recently been reported, based on explicit solutions for stationary symmetric self-similar MHD flows, stating that this type of shock transition is possible.[24] The other shock transitions present in the bow shock flow also belong to the theoretically predicted class of allowed shock transitions.[24] We can conclude that the flow configuration, characteristic analysis, and types of shock transitions of our interacting bow shock solution are illustrations and 2D extensions of many of the recent theoretical results obtained from analysis of stationary symmetric self-similar MHD flows.[24]

B. Steady MHD compound shocks

In Fig. 9(a) we show a plot of the pressure along the conducting plate close to the leading shock, and in Fig. 9(b) the pressure is plotted along a cut perpendicular to shock front EG (as indicated by the thin dotted line in Fig. 13). In both cases, the shock is followed by a clear rarefaction. This is topologically analogous to MHD compound shocks in the xt plane. We will now investigate if these structures are steady analogs of the xt compound shock. We will first review the characteristic properties of xt compound shocks by discussing a simple scalar example.[28]

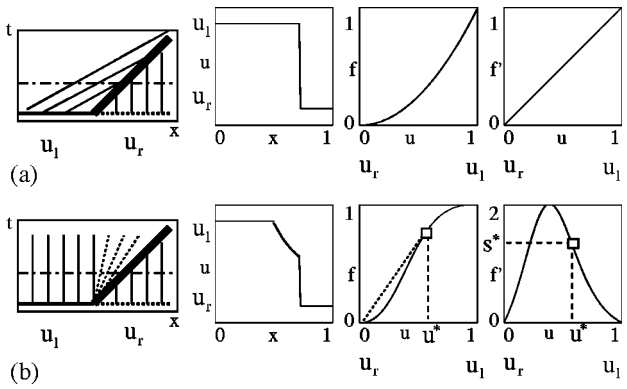

FIG. 10. (a) Solution of the Riemann problem for $u_l=1$ and $u_r=0$, with convex flux function $f(u)=u^2/2$. From left to right: The shock (thick) is admissible because the characteristics (thin) enter the shock; xu plot at the time indicated by the dash–dotted line in the leftmost picture; the flux function; the characteristic speed function. (b) Solution of the Riemann problem for $u_l=1$ and $u_r=0$, with nonconvex flux function $f(u)=u^2/(\frac{3}{2}u^2-u+\frac{1}{2})$. A single shock would not be admissible because characteristics would leave the shock. An intermediate state u^* can be found, which can be connected to u_r via a shock, and to u_l via a rarefaction. From left to right: The compound shock [shock (thick) with attached rarefaction (thin dotted); the characteristic in the rarefaction is parallel to the shock where the rarefaction is attached to the shock]; xu plot at the time indicated by the dash–dotted line in the leftmost picture; the flux function with the intermediate state u^*; the characteristic speed function.

The scalar nonlinear conservation law Eq. (3) allows for discontinuous solutions (shocks) that propagate with a speed s determined by the RH relation

$$s=\frac{f(u_r)-f(u_l)}{u_r-u_l}, \tag{34}$$

where u_r and u_l are the states on the right and the left of the discontinuity.[28]

Let us consider as a first example the flux function of the inviscid Burger's equation, viz., $f(u)=u^2/2$. This function $f(u)$ is called convex, as $f'(u)$ is monotone in u and $f''(u)$ does not change sign. In Fig. 10(a), we show how a Riemann problem with uniform left and right states $u_l=1$ and $u_r=0$, leads to a shock propagating with shock speed $s=\frac{1}{2}$. If we use for the moment the (naive, see below) geometrical shock admissibility condition that characteristics have to enter the shock, then this shock is an admissible shock solution. The characteristics on the left and right of the shock indeed enter the shock, as the shock speed s lies between $f'(u_l)$ and $f'(u_r)$, because $f(u)$ is convex.

Next, let us consider the flux function $f(u)=u^2/(\frac{3}{2}u^2-u+\frac{1}{2})$. This function is not convex, because $f'(u)$ is not monotone as can be seen in Fig. 10(b). For a Riemann problem with the same values $u_l=1$ and $u_r=0$, the shock speed

$s=1$ does not lie between $f'(u_l)$ and $f'(u_r)$. This is possible because $f(u)$ is not convex. This leads to an inadmissible shock, where the characteristics on the left of the shock, with characteristic speed $f'(u_l)=0$, would come out of the shock. An admissible solution for this Riemann problem can be found by extending the model to one involving compound shocks, which are shocks with an attached nonuniform region. An intermediate state u^* can be found, for which

$$f'(u^*)=\frac{f(u_r)-f(u^*)}{u_r-u^*}=s, \tag{35}$$

meaning that state u^* can be connected to u_r by a shock transition. On the left of the shock, the characteristic determined by $f'(u^*)$ will thus be parallel to the shock, and state u^* can be connected via a continuous rarefaction wave with the uniform state u_l. In the shock frame, $f'(u^*)=0$, and we say that the solution is sonic where the rarefaction is attached to the shock. A compound shock is thus a shock with a sonic rarefaction attached to it. This rarefaction is of a finite extent, moving with the same speed as the shock, but spreading out continuously in time.

At this point it is important to add some comments on the physical admissibility of shocks. For nonstrictly hyperbolic and nonconvex systems, the admissibility of shocks is quite complicated and the geometrical admissibility condition is not sufficient. So to be complete, the above discussed Riemann problem analysis based on nonconvexity of the ideal equations, has to be supplemented with an admissibility study based on models which take into account some of the physical effects that are left out in the ideal equations. Wu[33] studies the admissibility of shocks for a scalar nonconvex equation by including dissipative and dispersive terms, and finds numerically that the admissibility of the sonic shocks which are embedded in the above defined compound shocks, depends on the ratio of the dissipative and dispersive coefficients. For broad regions of the parameter space of the dissipative and dispersive coefficients, the conclusions from the ideal analysis remain valid, and compound shocks are admissible elements of solutions of Riemann problems, but for some parameter regions, the compound shocks do not occur.

The concept of a compound shock carries over to the separate nonconvex characteristic fields of systems of hyperbolic equations. In this case, the attached rarefaction will be a simple wave, with the consequence that one family of characteristics in the rarefaction will consist of straight lines.[12,14,18] The MHD flux function is not convex for the fast and the slow characteristic fields,[27] and compound shocks, with embedded sonic intermediate shocks, can occur in MHD.

The admissibility of MHD shocks can be studied in the MHD system with dissipative terms, and it is shown that the admissibility of intermediate MHD shocks can depend on the form of the dissipation.[29,30,33,34] It is argued that dissipative effects have to be taken into account in studying admissibility of MHD shocks, and that ''evolutionarity'' considerations, which are based on linear stability analysis of the ideal MHD equations, are insufficient to determine which MHD shocks can exist in physical reality.[29,30,33,34]

As was discussed in Sec. I, we can say that although there seems to be quite general agreement that MHD intermediate and compound shocks are theoretically admissible in the case of planar symmetry[11,30,33,34,44,45] ($B_z\equiv 0$ and $v_z\equiv 0$), Barmin *et al.*[44] and Falle *et al.*,[45] based on evolutionarity arguments, question if intermediate shocks can survive in simulations in the full MHD system with three vector components,[44,45] and if they can exist in the real world. Contrary to this, the theoretical results based on analysis of the dissipative MHD equations allow for intermediate shocks to persist for a considerable time in the real world, and possibly also for long times in special cases.[29,30,33–36,40] Wu[35,36] argues that intermediate shocks, when exposed to nonplanar perturbations, will decay into broad Alfvén waves. This would however not happen in an instantaneous disintegration, as predicted by the evolutionarity theory,[17,20] but in a continuous process involving time-dependent intermediate shocks. Wu[33] also shows that intermediate shocks can be formed through wave steepening of smooth initial profiles. It is thus conceivable that when intermediate shocks present in a 3D bow shock flow are perturbed by nonplanar perturbations and start to decay, this process can be reversed through wave steepening as soon as the perturbation has passed. Chao[41] claims the observation of an intermediate interplanetary shock. Observations of solar coronal mass ejections[42] reveal bright features which can be interpreted as shock fronts. Those shock fronts can have a peculiar geometry with a ''dimple,'' and this has been attributed to the possible presence of intermediate MHD shocks.[25,42,43]

Our bow shock simulation results are the first clear confirmation in 2D that intermediate shocks can indeed exist, at least in the reduced planar system. However, the question of the physical existence of intermediate and compound shocks in a nonplanar context can clearly not be addressed by our present planar simulation results. It is certainly interesting to examine these planar steady state simulation results to see if a steady analog for xt compound shocks can be identified. We have to realize, however, that it is not sure if the structures identified in this planar flow would survive in simulations of the full MHD system, and if they can exist in the real world, given the debate on the physical existence of intermediate shocks in a nonplanar context. Future extensions of our bow shock simulations to configurations in three space dimensions (3D) may be able to contribute to the answer to this question. It is important to note that we obtain a very similar topology with intermediate shocks for the axisymmetrical field-aligned flow over a sphere in the switch-on parameter regime.[26]

Myong and Roe[30] show analytically that all planar intermediate shocks—except the 2–3 shock—do have viscous profiles for the case where all the viscous parameters are equal, and that sonic intermediate shocks embedded in compound shocks are essential elements in the analytical solution of some planar xt MHD Riemann problems. They relate the occurrence of compound shocks in the planar case to the inadmissibility of 2–3 undercompressive intermediate shocks for which the compound shocks—with embedded sonic intermediate shocks—are substitutes. They theoretically predict the existence of double xt compound shocks,

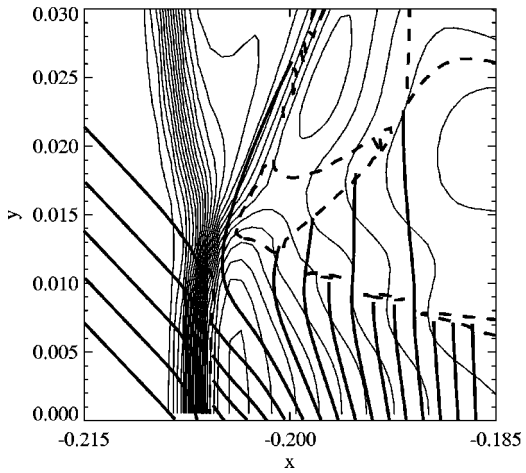

FIG. 11. First family of characteristics (thick solid) near the shock EF. The thin lines are density contours. The characteristics enter the shock, so this is not a compound shock.

composed of a fast rarefaction, followed by a $1=2-3=4$ sonic intermediate shock, followed by another slow rarefaction.

A steady compound shock should have the following properties, based on carrying over the geometry of characteristics from the xt case to the xy case. First, the flow should be hyperbolic on the two sides of the shock. Second, the shock should have a rarefaction attached to it which is a simple wave with one family of characteristics consisting of straight lines. Third, the xy characteristics should be parallel to the shock in the xy plane, such that the flow is sonic in the xy plane where the shock is attached to the rarefaction. We will now investigate several wave structures in the simulated bow shock flow to see if they fulfill these criteria.

We start with the leading shock at the conducting plate. Fig. 9(a) suggests that this could be a steady compound shock. Figure 8 confirms that the flow is hyperbolic on both sides of the shock, but the behavior of the two characteristic families shown in Figs. 11 and 12, shows that this is not a steady compound shock as we have defined above. Neither

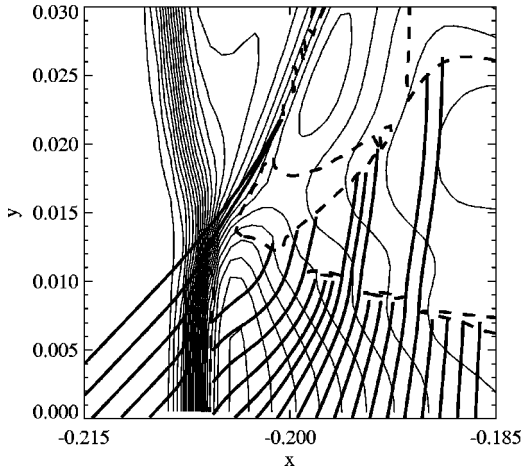

FIG. 12. Second family of characteristics (thick solid) near the shock EF. The thin lines are density contours. The characteristics enter the shock, so this is not a compound shock.

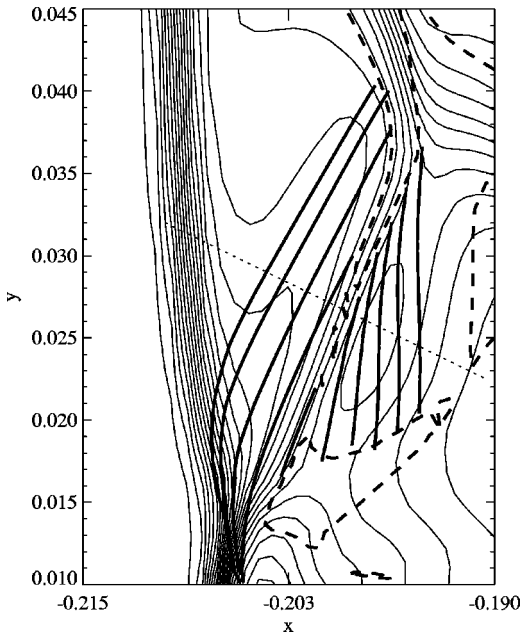

FIG. 13. First family of characteristics (thick solid) near the intermediate shock EG. The thin lines are density contours. The characteristics become parallel to the shock on the left and are straight lines, so this is a compound shock.

of the characteristics is parallel to the shock where the rarefaction is attached to the shock, and the two families are not straight but interact in the rarefaction which is thus not a simple wave. This conclusion is consistent with the discussion in DSLP98, where it was shown that this rarefaction is a 2D effect associated with the converging flow behind the shock. The plasma speed equals neither of the wave speeds where the rarefactions are attached to the shock, as was shown in Figs. 8(f)–8(h) of DSLP98.

Figures 11 and 12 also reveal another interesting phenomenon. As the pressure in the rarefaction in Fig. 9(a) drops when going to the right, the characteristics in Figs. 11 and 12 straighten and form one coinciding limiting characteristic where the pressure reaches a constant state after the rarefaction (at $\sim x=-0.185$). This limiting characteristic is allowed because the streamlines are perpendicular to it. This limiting line is a locus of weak discontinuity, where the pressure is continuous, but the slope of the pressure has a discontinuity. This weak discontinuity connects the rarefaction region with the uniform flow region behind it, and Fig. 8(g) of DSLP98 shows that the flow is indeed sonic at the location of this weak discontinuity. The rarefaction region bordering the uniform region is, however, not a simple wave region, such that this special configuration with a limiting characteristic seems to be an exception to the rule that a uniform region in a stationary 2D flow can only be bordered by a simple wave region.[14]

We now turn our attention to intermediate shock EG. Figures 9(b)–9(d) suggest that this could be a steady compound shock with an embedded $1=2-3=4$ intermediate shock. The behavior of the two characteristic families shown in Figs. 13 and 14, shows that the flow is hyperbolic on both sides of the shock. The second family of characteristics (Fig.

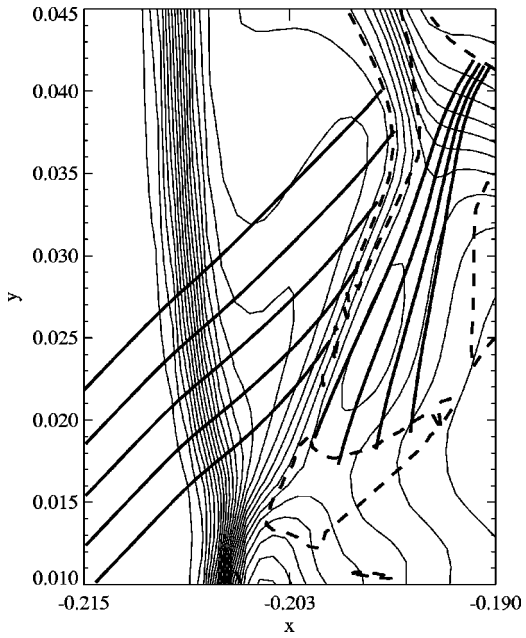

FIG. 14. Second family of characteristics (thick solid) near the intermediate shock EG. The thin lines are density contours. The characteristics become parallel to the shock on the right and are straight lines, so this is a compound shock.

14) is parallel to the shock on the right, and goes into the shock on the left. The characteristics of this family are straight on the right of the shock, indicating a simple centered slow rarefaction wave with the characteristics apparently converging in point G. The first family of characteristics (Fig. 13) is parallel to the shock on the left (with straight lines), and goes into the shock on the right. The characteristics of this family are straight on the left of the shock. The intermediate shock is thus preceded and followed by simple rarefaction waves which are sonic at the point where they are attached to the shock. This rarefaction–shock–rarefaction structure has thus all the defining properties of a compound shock. This compound shock is sonic on the two sides, so we can call this newly identified steady wave structure a *double steady compound shock* [Fig. 15(b)]. Such a structure has been predicted theoretically recently in the context of xt compound shocks[30] [Fig. 15(a)]. It has not been identified yet in xt simulations, but it is noteworthy that we encounter the analogous steady xy structure in our 2D simulation results. This new steady structure is a manifestation of the nonconvex nature of the MHD equations, just like the sonic intermediate shocks embedded in xt time dependent compound shocks are a manifestation of this property. We have thus established by explicit example a remarkably complete analogy between the characteristic structure of time-dependent compound waves in the xt plane and the characteristic structure of steady compound waves in the xy plane. Following Myong and Roe,[30] we can argue that this steady compound shock occurs as a substitute for a 2–3 intermediate shock which is undercompressive in the planar case.

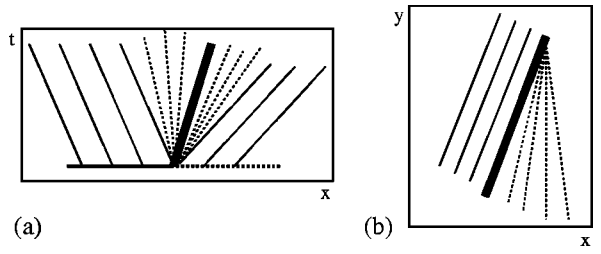

FIG. 15. (a) Sketch of the recently theoretically predicted double xt compound shock. The shock (thick) is preceded and followed by rarefactions (thin dotted), which are attached to the shock with characteristics parallel to the shock. (b) Sketch of the topology of the characteristics near the double xy compound shock which is present in our simulation results. The shock (thick) is preceded and followed by simple wave rarefaction regions, which are attached to the shock with straight characteristics parallel to the shock.

We suggest the following physical relationship between the two kinds of compound shocks, those of time-dependent flows in the xt plane and those of steady flows in the xy plane. If an initial plane compound shock taken in the time-dependent sense and moving in xyt space with a sonic fast rarefaction (which is expanding in time) attached to it, were to slow down and become steady, then such a structure could conceivably retain the property that the now steady rarefaction is sonic ($v_\perp = c_{f\perp}$) at the point where it is attached to the shock. This is precisely the defining property of a fast characteristic in steady xy space (see Sec. II), which means that all the points at the locus where the rarefaction is attached to the shock with a sonic speed, will lie on a steady xy characteristic parallel to the shock, thus explaining that the steady xy characteristic will be parallel to the shock where the rarefaction is attached to it. This observation clarifies a natural relationship between xt and xy compound shocks, which could possibly be further explored by explicit numerical simulation of the above proposed scenario. It also explains why the flow in terms of xt wave speeds is sonic where the rarefactions are attached to the shocks in steady compound shocks, as can be seen in Figs. 9(c) and 9(d).

VII. SUMMARY AND CONCLUSION

In this paper we have presented a concise and systematic derivation of some aspects of the characteristic theory of the MHD equations, and then we have applied this characteristic analysis to a complex field-aligned MHD bow shock flow with interacting shocks.

We have started out with an instructive presentation of the characteristic theory of the MHD equations with two independent variables, based on the symmetrizable Galilean invariant form of the equations and using a matrix approach. Our derivation is attractive because it is simple and systematic. The characteristic structure derived from the symmetrizable form of the MHD equations turns out to be consistent and complete, without the need to impose the $\nabla \cdot \mathbf{B} = 0$ constraint.

We have then analyzed the bow shock flow in terms of characteristics, elliptic and hyperbolic regions, limiting lines, and allowed shock transitions. Our results are an illustration and a 2D extension of many of the recent theoretical results on characteristic structure and allowed shock transitions that were obtained from analysis of stationary symmetric self-similar MHD flows.[24]

This analysis in terms of characteristics and elliptic and hyperbolic regions gives insight into the global topology of the bow shock flow and into the flow of information in the bow shock solution. A more important result of our analysis is, however, the discovery of planar 2D steady state MHD wave structures that are exact mathematical analogs of the MHD compound shocks encountered in planar 1D time-dependent flows. We have shown that the interacting bow shock flow contains a structure composed of a fast simple wave rarefaction, followed by a sonic intermediate shock, followed by a slow simple wave rarefaction. Analysis of the characteristics in the steady xy plane, shows that this structure has all the mathematical properties of the compound shock that was previously studied in the context of planar 1D time-dependent MHD flows. We have thus established a complete analogy between the characteristic structure of time-dependent compound waves in the xt plane and the characteristic structure of the newly discovered steady compound waves in the xy plane. Even more significant is that this structure turns out to be the steady analog of the double compound shock that has been predicted theoretically recently in the context of xt MHD compound shocks.[30] We suggested that this novel steady compound wave can be the terminal state of its time-dependent counterpart as an initially time-dependent 1D flow relaxes to a 2D steady state. Our findings are thus a new manifestation of the wealth of interesting wave effects that are described by the MHD equations. It is important to be aware, however, that it remains to be seen if the intermediate and compound shocks present in our 2D planar simulation results, would survive in the more general full MHD system which allows for nonplanar perturbations, given the debate on the physical existence of intermediate shocks in a nonplanar context.

Our study of the bow shock flow shows that characteristic analysis is a powerful tool that can give insight into complex nonlinear flows, and this approach may be useful to analyze numerically obtained solutions for solar and stellar winds and other astrophysical flows.[53]

Future work will include analysis of flow characteristics and wave structures in 3D flows, where the field does not have to be aligned with the flow. The possible formation and properties of intermediate and compound shocks in 3D space is an interesting and highly debated topic, and the complicating factor of noncoplanarity and stability to nonplanar perturbations enters automatically in a 3D configuration.[30,33–36,40,44,45] These extensions of our bow shock simulations to configurations in three space dimensions may be able to contribute to the answer to the question of the physical existence of intermediate shocks. Together with DSLP98, the present article will serve as a reference for this future 3D work. Time-dependent simulations of this kind of shock interaction processes will be performed in the context of solar coronal mass ejections.[25] The intricate MHD wave structures that are present in our simulation results, may be observed in space plasmas with coronagraph observations[42,43] or *in situ* satellite observations.[57]

ACKNOWLEDGMENTS

This work derives from the Ph.D. thesis research of H.D.S. carried out at the High Altitude Observatory, National Center for Atmospheric Research, Boulder, Colorado, USA, and at the Center for Plasma Astrophysics, K. U. Leuven, Belgium. H.D.S. was supported by a HAO Newkirk Research Assistantship. H.D.S. acknowledges helpful discussions with K. MacGregor, A. Hundhausen, H. Deconinck, A. Csík, R. S. Myong, K. G. Powell, P. L. Roe, K. C. Hansen, T. J. Barth, S. Komissarov, C. Rohde, and H. Freistuehler. The National Center for Atmospheric Research is sponsored by the National Science Foundation (USA).

[1] L. D. Landau and E. M. Lifshitz, *Electrodynamics of Continuous Media* (Pergamon, Oxford, 1984).
[2] E. Priest, *Solar Magnetohydrodynamics*, *Geophysics and Astrophysics Monographs* (Reidel, Dordrecht, 1982).
[3] T. Sakurai, Comput. Phys. Rep. **12**, 247 (1990).
[4] K. Tsinganos, C. Sauty, G. Surlantzis, E. Trussoni, and J. Contopoulos, Mon. Not. R. Astron. Soc. **283**, 811 (1996).
[5] B. C. Low, Sol. Phys. **167**, 217 (1996).
[6] T. J. Linde, T. I. Gombosi, P. L. Roe, K. G. Powell, and D. L. De Zeeuw, J. Geophys. Res. **103**, 1889 (1998).
[7] D. Biskamp, *Nonlinear Magnetohydrodynamics* (Cambridge University Press, Cambridge, 1993).
[8] S. Poedts, W. Kerner, J. P. Goedbloed, B. Keegan, G. T. A. Huysmans, and E. Schwarz, Plasma Phys. Controlled Fusion **34**, 1397 (1992).
[9] H. De Sterck, S. Poedts, and J. P. Goedbloed, J. Plasma Phys. **59/2**, 277 (1998).
[10] R. Courant and D. Hilbert, *Methods of Mathematical Physics* (Interscience, New York, 1962), Vol. 2.
[11] J. E. Anderson, Ph.D. thesis, M. I. T., 1963.
[12] M. A. Liberman and A. L. Velikovich, *Physics of Shock Waves in Gases and Plasmas, Vol. 19* of *Springer Series in Electrophysics* (Springer-Verlag, Berlin, 1985).
[13] H. De Sterck, B. C. Low, and S. Poedts, Phys. Plasmas **5/11**, 4015 (1998).
[14] R. Courant and K. O. Friedrichs, *Supersonic Flow and Shock Waves* (Interscience, New York, 1948).
[15] Y. Kato and T. Taniuti, Prog. Theor. Phys. **21**, 606 (1959).
[16] H. Grad, Rev. Mod. Phys. **32**, 830 (1960).
[17] A. Jeffrey and T. Taniuti, *Non-linear Wave Propagation* (Academic, New York, 1964).
[18] A. G. Kulikovskiy and G. A. Lyubimov, *Magnetohydrodynamics* (Addison-Wesley, Reading, MA, 1965).
[19] A. Jeffrey, *Magnetohydrodynamics* (Oliver & Boyd, Edinburgh, 1966).
[20] A. I. Akhiezer, I. A. Akhiezer, R. V. Polovin, A. G. Sitenko, and K. N. Stepanov, *Plasma electrodynamics* (Pergamon, Oxford, 1975), Vol. 1.
[21] M. Heinemann and S. Olbert, J. Geophys. Res. **83**, 2457 (1978).
[22] J. Contopoulos, Astrophys. J. **460**, 185 (1996).
[23] A. Lifshitz and J. P. Goedbloed, J. Plasma Phys. **58**, 61 (1997).
[24] J. P. Goedbloed and A. Lifshitz, Phys. Plasmas **4**, 3544 (1997).
[25] R. S. Steinolfson and A. J. Hundhausen, J. Geophys. Res. **95**, 6389 (1990).
[26] H. De Sterck and S. Poedts, to appear in Astron. Astrophys. (1999).
[27] M. Brio and C. C. Wu, J. Comput. Phys. **75**, 400 (1988).
[28] R. J. Leveque, *Numerical Methods for Conservation Laws, Lectures in Mathematics ETH Zurich* (Birkhauser-Verlag, Basel, 1992).
[29] R. S. Myong and P. L. Roe, J. Plasma Phys. **58**, 485 (1997).
[30] R. S. Myong and P. L. Roe, J. Plasma Phys. **58**, 521 (1997).
[31] C. C. Wu, J. Geophys. Res. **95**, 8149 (1990).
[32] C. F. Kennel, R. D. Blandford, and C. C. Wu, Phys. Fluids B **2**, 253 (1990).
[33] C. C. Wu, in *Viscous Profiles and Numerical Methods for Shock Waves, Siam Proceedings Series*, edited by M. Shearer (SIAM, Philadelphia, 1991), pp. 209–236.
[34] H. Freistuehler, J. Geophys. Res. **96**, 3825 (1991).
[35] C. C. Wu and C. F. Kennel, Phys. Rev. Lett. **68**, 56 (1992).

[36]C. C. Wu and C. F. Kennel, Geophys. Res. Lett. **19**, 2087 (1992).
[37]H. Freistuehler and P. Szmolyan, SIAM (Soc. Ind. Appl. Math.) J. Math. Anal. **26**, 112 (1995).
[38]H. Freistuehler, in *Nonlinear Evolutionary Partial Differential Equations*, edited by X.-X. Ding and T.-P. Liu (American Mathematical Society and International Press, 1997), pp. 175–187.
[39]H. Freistuehler, Phys. Scr. **T74**, 26 (1998).
[40]R. S. Myong and P. L. Roe, J. Comput. Phys. **147**, 545 (1998).
[41]J. K. Chao, Adv. Space Res. **15**, 521 (1995).
[42]A. J. Hundhausen, in *The Many Faces of the Sun*, edited by K. T. Strong, J. L. R. Saba, B. M. Haisch, and J. T. Schmelz (Springer-Verlag, New York, 1998), pp. 143–200.
[43]H. De Sterck, H. Deconinck, S. Poedts, and D. Roose, in *Proceedings of the Seventh International Conference on Hyperbolic Problems* (Birkhauser-Verlag, Basel, 1999) (in press).
[44]A. A. Barmin, A. G. Kulikovskiy, and N. V. Pogorelov, J. Comput. Phys. **126**, 77 (1996).
[45]S. A. E. G. Falle, S. S. Komissarov, and P. Joarder, Mon. Not. R. Astron. Soc. **297**, 265 (1998).
[46]S. A. Markovskii, Phys. Plasmas **5**, 2596 (1998).
[47]P. A. Thompson, *Compressible-Fluid Dynamics* (McGraw-Hill, New York, 1972).
[48]S. K. Godunov, in *Nonlinear Hyperbolic Problems: Proceedings of an Advanced Research Workshop, Lecture Notes in Mathematics, Vol. 1270*, edited by C. Carasso, P.-A. Raviart, and D. Serre (Springer-Verlag, Berlin, 1987).
[49]K. G. Powell, P. L. Roe, R. S. Myong, T. I. Gombosi, and D. L. De Zeeuw, AIAA Paper **95-1704-CP** (American Institute of Aeronautics and Astronautics, Washington DC, 1995).
[50]T. J. Barth, in *An Introduction to Recent Developments in Theory and Numerics for Conservation Laws, Lecture notes in Computational Science and Engineering*, edited by D. Kröner, M. Ohlberger, and C. Rohde (Springer-Verlag, Berlin, 1998), pp. 195–284.
[51]J. U. Brackbill and D. C. Barnes, J. Comput. Phys. **35**, 426 (1980).
[52]G. Tóth and D. Odstrcil, J. Comput. Phys. **128**, 82 (1996).
[53]R. Keppens and J. P. Goedbloed, to appear in Astron. Astrophys. (1999).
[54]G. B. Whitham, *Linear and Nonlinear Waves* (Wiley, New York, 1974).
[55]L. M. Sarro, H. De Sterck, R. Erdélyi, B. Montesinos, and J. G. Doyle, in *Proceedings of the Fifth SOHO Workshop* (ESA SP-404, European Space Agency, Paris, 1997), pp. 657–661.
[56]L. M. Sarro, J. G. Doyle, B. Montesinos, R. Erdélyi, and H. De Sterck, in *The Tenth Cambridge Workshop on Cool Stars, Stellar Systems and the Sun*, edited by R. A. Donahue and J. A. Bookbinder (Astronomical Society of the Pacific, ASP Conf. Ser. 154, 1998), p. 693.
[57]N. R. Sheeley, Jr., R. A. Howard, D. J. Michels, M. J. Koomen, R. Schwenn, K. H. Muehlhaeuser, and H. Rosenbauer, J. Geophys. Res. **90**, 163 (1985).